ORIGINAL RESEARCH

Effects of Uremic Clearance Granules on p38 MAPK/NF-κB Signaling Pathway, Microbial and Metabolic Profiles in End-Stage Renal Disease Rats Receiving Peritoneal Dialysis

Xiaosheng Li[1], Jie Zheng[1], Jian Wang[1], Xianhu Tang[1], Fengxia Zhang[1], Shufeng Liu[1], Yunqiang Liao[2], Xiaoqing Chen[1], Wenjuan Xie[1], Yang Tang [ID][3]

[1]Department of Nephrology, The First Affiliated Hospital of Gannan Medical University, Ganzhou, 341000, People's Republic of China; [2]First Clinical Medical College of Gannan Medical University, Ganzhou, 341000, People's Republic of China; [3]Department of Traditional Chinese Medicine, The First Affiliated Hospital of Gannan Medical University, Ganzhou, 341000, People's Republic of China

Correspondence: Yang Tang, Department of Traditional Chinese Medicine, The First Affiliated Hospital of Gannan Medical University, Qingnian Road, Suite 23, Ganzhou, 341000, People's Republic of China, Email tangyangtcm@gmu.edu.cn

Background: End-stage renal disease (ESRD) is the final stage of chronic kidney disease (CKD). In the clinic, Uremic Clearance Granules (UCG) are mainly used in the treatment of early CKD and stabilized renal function. However, the benefits and mechanisms of UCG on ESRD remain unclear.

Methods: Rats were randomly divided into four groups: sham group, model group, peritoneal dialysis (PD) group and UCG group. Except for the sham-operated group, ESRD was induced by 5/6 nephrectomy in the other three groups. The PD group and UCG group were then subjected to PD. In addition, the UCG group was given UCG by gavage when PD. Changes in body weight and final kidney weight of rats in each group were monitored. HE and Masson staining were performed to confirm the extent of renal fibrosis. Biochemical kits were used to detect blood urea nitrogen (BUN), serum and urine creatinine (Scr, Cre), and urine protein (UPr) levels. ELISA was used to detect the rats' inflammatory responses. qRT-PCR, WB, and IHC were probed to determine the expression levels of NF-κB and MAPK. 16S rDNA sequencing was performed to analyze the composition of gut microbiota in rats. A liquid chromatograph-mass spectrometer was performed to reveal serum metabolomics changes.

Results: UCG increased renal volume and body weight, improved renal fibrosis. It enhanced renal function and decreased the levels of BUN, Scr, Upr, Cre, inflammatory responses, as well as NF-κB and MAPK expressions in renal and colon tissues of ESRD rats. The relative abundances of Bacteroidetes and Firmicutes changed in ESRD rats in response to UCG. Serum metabolomics was utilized to identify 70 differentiated metabolites, which were associated with D-glutamine and D-glutamate metabolism, and Phenylalanine metabolism.

Conclusion: Our study confirmed that UCG alleviated ESRD by regulating p38 MAPK/NF-κB signaling pathway, microbial and metabolic profiles.

Keywords: end-stage renal disease, uremic clearance granules, gut microbiota, p38 MAPK/NF-κB signaling pathway

Introduction

End-stage renal disease (ESRD), the fifth and final stage of chronic kidney disease (CKD), is characterized by a gradual and irreversible loss of kidney function as toxins build up in the body. Its common symptoms include breathing difficulties, nausea, pain, fatigue, sleep disturbances, anxiety and depression.[1,2] There are two main treatments for ESRD of peritoneal dialysis (PD) and hemodialysis (HD). More than 2.5 million people with ESRD require maintenance of dialysis worldwide.[3] Currently, PD technology has been widely used in the long-term treatment of ESRD, and treatment-related complications have been greatly reduced.[4] However, there are still some problems such as unsatisfactory effects in PD therapy. For example, patients receiving PD are more prone to peritonitis, cardiovascular disease, hyperglycemia, etc

[PMC5084899]. Therefore, it is urgent to find some auxiliary means, such as drug therapy, to improve the therapeutic efficiency of PD in the treatment of ESRD.

Uremic Clearance Granules (UCG, Niaoduqing Keli in Chinese) is the most common Chinese herbal medicine in the field of therapy of CKD.[5] Huang et al showed that UCG alleviated renal dysfunction and tubulointerstitial fibrosis by promoting extracellular matrix degradation in CKD rats.[6,7] Meiwu et al found that UCG showed a positive effect on delaying renal function decline of CKD by reducing serum creatinine (Scr) and creatinine clearance rate (Ccr).[8] So far, there are few reports on the effects of UCG on ESRD. But as the final stage of CKD, UCG is highly likely to alleviate ESRD. The mitogen-activated kinase (MAPK) family could control cell adaptation to stress stimuli.[9] The nuclear factor kappa B (NF-κB) is a transcription factor family involved in cytokine production, inflammatory response, and cancer development. Its activation could lead to the release of pro-inflammatory cytokines such as TNFα and IL-1β.[10,11] P38 (one of MAPK) targets P65 (one of NF-κB) and is involved in regulating the expression of several genes responsible for the progression of various inflammatory diseases.[12,13] For example, hydrogen sulfide improved chronic renal failure in rats by inhibiting apoptosis and inflammation through the ROS/MAPK and NF-κB signaling pathways.[14] Long non-coding RNA MANTIS could alleviate the injury of protein-bound uremic toxin in human umbilical vein endothelial cells (HUVECs) through p38 MAPK and p65 NF-κB pathways in ESRD.[15] Renal fibrosis is the common result of almost all CKD and is always accompanied by an active inflammatory response.[16] Researchers suggest that UCG could significantly reduce glomerulosclerosis and renal tubulointerstitial fibrosis in 5/6 nephrectomized rats.[17] Therefore, we speculate that UCG might alleviate ESRD through p38 MAPK/NF-κB signaling pathway.

The interaction between the gut and the kidney is known as the "gut-renal axis", of which gut microbiota is an important part.[18] Gut dysbacteriosis refers to the state of abnormal microbiota diversity and richness, which may lead to immune, metabolic, or endocrine disorders, and aggravate the development of CKD.[19] Significant differences in the abundance of 190 bacterial operational taxonomic units (OTUs) between healthy person and ESRD patients have been reported by Nosratola D Vaziri.[20] Compared with healthy people, the total number of bacteria in the stool of ESRD patients was appreciably raised.[20] The enterotypes of ESRD patients changed from Prevotella to Bacteroides, and the gut microbiota was associated with the inflammatory state and renal function of CKD.[21] However, no literature has revealed the effects of UCG on gut microbiota and microbial metabolism in ESRD patients, and its potential specific mechanism remains to be explored.

In this study, 5/6 nephrectomy models in rats were established. We conducted molecular experiments, 16S rDNA sequencing and liquid chromatograph-mass spectrometer (LC-MS) to explore whether and how UCG could improve the effect of PD on ESRD. Our study is expected to improve the understanding of the pathogenesis of ESRD and the mechanism of UCG in treating ESRD. It provides a basis for us to seek new targets and strategies for treating ESRD.

Materials and Methods
Animal Models
Twenty-five 12-week-old male Sprague-Dawley (SD) rats weighing 180–200 g were purchased from Hunan Sja Laboratory Animal Co., Ltd. This study was approved by First Affiliated Hospital of Gannan Medical University Ethics Committee (No.LLSC-2021052101). The research was carried out in compliance with the Guiding Opinions on the Treatment of Laboratory Animals (issued by the Ministry of Science and Technology of the People's Republic of China) and the ARRIVE guidelines. All animals were kept in an environmentally controlled room at 24° C ± 2° C, with a relative humidity of 55% ± 5%, and subjected to a 12-hour light/dark cycle. Food and water are freely available. After one week of feeding, 5 rats that only opened the abdominal cavity without removal of kidneys were named as Sham group. Another 20 rats underwent a 5/6 nephrectomy (5/6 Nx). Briefly, the left 2/3 kidneys of the rats were removed. After one week, the right kidneys of the remaining surviving rats were completely removed. One week after surgery, the levels of blood urea nitrogen (BUN) and serum creatinine (Scr) in the serum of the remaining surviving rats were detected. If the levels were twice that of the Sham group, the 5/6 Nx model was successful. 5/6 Nx mice were randomly divided into 3 groups (n=5 in each group): Model group, PD group, and UCG group. A peritoneal dialysis tube was inserted into the retroperitoneal cavity of the rats in the PD group and the UCG group. Then, 4.25% glucose peritoneal dialysis solution (H20133286, Baite) (100 mL/kg/d) was injected into the abdominal cavity.[22] At the same time of PD, the rats in the UCG group were gavaged with UCG (5 g/kg/d) (CONSUN Pharmaceutical Co., Ltd.).[6] Rats in the Sham

group and Model group were gavaged with the same volume of saline. After 4 weeks of treatment, each rat was fasted and placed in separate metabolic cages to collect urine and fecal samples for 24 h. The manual cervical dislocation method was used to euthanize rats. Serum was collected by abdominal aortic puncture under anesthesia. Residual renal and colon tissue was stored for further testing.

Quantity Control of UCG

The HPLC-fingerprint of UCG has been reported by Dr. Huang et al.[6] We also performed HPLC on UCG. Briefly, 2g of UCG particles were dissolved in 50mL of water. 100 μL of solution and 400 μL of extract solution (methanol: acetonitrile=1:1) were mixed for 10 min. It was then sonicated at 4°C for 5 min. The samples were then placed at −20°C for 1 h, and the supernatant was collected by centrifugation. After draining with a freeze concentrator, we added 200uL of dissolving solution (acetonitrile: water=1:1) to reconstitute it. The samples were analyzed using liquid chromatograph-mass spectrometer (LC-MS).

Metabolomics Data Analysis

Rat serum was collected and assayed for metabolites with molecular weights less than 1000. The 100 μL plasma was mixed with 300 μL methanol and 20 μL internal standard (2-Chloro-L-phenylalanine, 103616-89-3, Hengbai). The mixture was placed in a sonicator for 5 min and then at −20 °C for 2 h. After being centrifuged at 13,000 rpm at 4 °C for 15 min, 200 μL supernatant was taken into a 2 mL injection flask for LC-MS analysis.

LC-MS

The instrument platform for LC-MS analysis consisted of the Agilent 1290 ultra-performance liquid chromatography in tandem with Thermo Fisher Scientific's Q ExActive Orbitrap High-Resolution Mass Spectrometer. The chromatographic column was the UPLC HSS T3 column (1.7 μm 2.1×100 mm, Waters). The Q ExActive Orbitrap High-Resolution Mass Spectrometer (Thermo Fisher Scientific, USA) was used to collect the primary and secondary mass spectrum data. Compound Discover (Version 2.0, Thermo) and OSI-SMMS (Version 1.0, Dashuo) software were applied in collaboration with the mzCloud database and self-built database for material identification. Finally, the normalized data matrix was used for multivariate statistical analysis and differential metabolites were screened.

Hematoxylin-Eosin (HE) Staining

Renal tissues preserved in 10% neutral buffer formalin solution were removed and embedded in paraffin. The samples were then cut into 4 μm thick slices and placed on glass slides (AY89-2, Yuantai). The samples were dewaxed with xylene and rehydrated with ethanol solutions of various concentrations. Next, they were stained with hematoxylin for 5 min and eosin for 2 min, respectively.[23] After elution with a multi-step concentration gradient of ethanol, the sections were sealed with neutral gum and observed under a microscope (BA210T, Motic).

Masson Staining

Follow the instructions of Masson staining kit (Abiowell, AWI0267a, China). After dewaxed and rehydrated, renal tissue sections were stained with Weigert's iron hematoxylin solution for 10 min. Then, the samples were washed with distilled water and stained with acid fuchsin solution for 15 min. The samples were incubated with 1% phosphomolybdate aqueous solution and blue aniline solution for 5 min. The samples were differentiated with 1% acetic acid solution for 1 min. After 95% alcohol dehydration, sections were sealed with neutral gum, observed and photographed under a microscope.

Enzyme-Linked Immunosorbent Assay (ELISA)

The levels of blood urea nitrogen (BUN), serum and urine creatinine (Scr, Cre), urinary protein (UPr), TNFα, IL1β, IL-5 and IL-6 in serum and urine of rats were determined by ELISA. All steps were strict to the instructions. After completing the last step, the absorbance at the specified wavelength was detected using a multifunctional enzyme-labeled analyzer (MB-530, Heales) within 5 min. The serum and urinary creatinine were measured by the creatinine kit (#C011-2-1, Jiancheng) and the Creatinine clearance rate (Ccr= Cre × urine volume per minute/Scr) was calculated accordingly. The

BUN kit (#C013-1-1), and UPr kit (#C035-2-1) were purchased from Nanjing Jiancheng Bioengineering Institute. Sino-American Biotechnology Co., Ltd provided the TNFα kit (#CSB-E11987r), IL1β kit (#CSB-E08055r), IL-5 kit (#CSB-E07435r), and IL-6 kit (#CSB-E04640r).

Quantitative Reverse Transcriptase-Polymerase Chain Reaction (qRT-PCR)

The relative expression levels of P65 and P38 in renal and colon tissues were detected by qRT-PCR. Total RNA of renal tissue was extracted by Trizol (15596026, Thermo). cDNA was obtained by reverse transcription using the total RNA of renal tissue as a template. The reverse transcription kit was purchased from Beijing Cwbio. The primers of the target gene were designed by Primer5 software (Table 1) and synthesized by Shanghai Sangon Biotech. Then, the PCR reaction was performed with a fluorescent quantitative PCR analyzer (PIKORALE96, Thermo), and real-time detection of fluorescence signals was performed during the process. β-actin was used as an internal reference, and the ratio of the target gene expression level of each sample to that of the control group was calculated by $2^{-\Delta\Delta\ CT}$ method (the Sham group was used as the control group in this experiment).

Western Blot (WB)

The expression levels of P65, p-P65, P38, and p-P38 in renal tissues and colon tissues were detected by WB. RIPA lysate (AWB0137a, Abiowell) was performed to extract total proteins from renal tissues. The protein solution was mixed with 5×Loading Buffer and then washed in water for 5 min. 10 μL protein samples were added to each well of the gel. Electrophoresis was performed at a constant voltage of 75 V for 130 min. After the completion of electrophoresis, the gel block containing the target proteins were cut out according to the instructions of a marker. Proteins in the gel were transferred to the nitrocellulose carbon film at a constant current of 300 mA. The membranes were sealed with 5% skim milk powder for 90 min. Then, the membranes were incubated with the primary antibody P65 (66535-1-Ig, 1:1000, proteintech), p-P65 (#3033, 1:1000, CST), P38 (14064-1-AP, 1:1000, proteintech), and p-P38 (12874-1-AP, 1:600, proteintech) at 4°C overnight. On the second day, the membranes were incubated with the secondary antibody HRP goat anti-mouse IgG (SA00001-1, 1:5000, proteintech) and HRP goat anti-rabbit IgG (SA00001-2, 1:6000, proteintech) for 90 min. Finally, the protein bands were visualized by ECL Plus luminescent solution (K-12045-D50, Advansta).

Immunohistochemistry (IHC)

The renal tissues and colon tissues of rats were embedded in paraffin and cut into 4 μm thick sections. The sections were successively placed in xylene and ethanol to dewax and rehydrate. Then, they were dipped in 0.01M citrate buffer (pH6.0) and microwaved to repair the antigen. 3% H_2O_2 was used to inactivate endogenous enzymes. The sections were then incubated with primary antibody P65 (ab32536, 1:200, Abcam) and P38 (ab31828, 1:200, Abcam) at 4°C overnight. On the second day, the sections were incubated with the secondary antibody at 37°C for 30 min. Next, the sections were stained with DAB and hematoxylin, sealed with neutral gum and observed under a microscope. The images were analyzed by Image-Pro-Plus (Media Cybernetics) software.

Table 1 qRT-PCR Primer Sequences

Gene	Sequences (5'-3')	Product Length (bp)
P65	F: CACCAAAGACCCACCTCACCG	155
	R: CTTGCTCCAGGTCTCGCTTC	
P38	F: AGCTTACCGATGACCACGTT	188
	R: CACGTAGCCGGTCATTTCGTC	
β-actin	F: ACATCCGTAAAGACCTCTATGCC	223
	R: TACTCCTGCTTGCTGATCCAC	

16S rDNA Sequencing

16S rDNA sequencing was applied to detect microbial diversity in 20 rat fecal samples. Microbial genomic DNA was extracted from fecal samples using the QIAAMP ® Fast DNA Stool Mini Kit (QIAGEN). Illumina Novaseq PE250 was performed to sequence 16S amplicon, and the primers were CCTACGGGNGGCWGCAG and GACTACHVGGGTATCTAATCC. The SILVA-132-99 database was conducted for reference. The QIIME 2 analysis process was used to call DADA2 to de-noise and de-redundancy the Raw Data and obtain Feature information. Species annotations were made for each amplicon sequence variant (ASV) sequence to obtain the corresponding species information and species-based abundance distribution (ie, ASV_TABLE). Species richness and evenness in the samples were analyzed based on ASV_TABLE, and differences in community structure among different groups were analyzed.

Statistical Analysis

We present all data as mean ± standard deviation (SD). Experimental data were analyzed using Graphpad Prism 8.0. One-way ANOVA was applied to compare differences between more than two groups. Wald test was performed to screen differential bacteria. Adonis and Anosim analyses were used to visualize differences in the abundance of major strains between groups. The differences between the two groups were analyzed by the Wilcox rank-sum test, and the differences between multiple groups were compared by the Kruskal–Wallis test to determine whether the differences in β diversity index within each group were significant. $P<0.05$ was considered statistically significant. Each experiment was repeated at least 3 times in this study.

Results

Composition Identification of UCG

The UCG used in this study was in granular form and was purchased from CONSUN Pharmaceutical Co., Ltd. It has been used in the clinical treatment of chronic kidney disease. Its quality stability has been tested by Prof. Quan et al.[6] Of course, we also detected its main components using LC-MS. The components obtained by LC-MS were arranged in descending order according to the size of the peak area. The substances with a large peak area in both positive and negative ion modes were mainly glycyrrhizic acid ammonium salt, albiflorin, paeoniflorin, and 2,3,5,4'-tetrahydroxystilbene-2-O-β-D-glucoside (TSG) (Supplementary Figure 1 and Supplementary Table 1).

UCG Alleviated the Symptoms of ESRD Rats

In this study, ESRD rats were used to investigate the effects of UCG in vivo. Figure 1A and B showed that compared with the Sham group, the kidney volume and body weight of rats in the Model group were significantly decreased. Compared with the Model group, the kidney volume and body weight in the PD group were increased. Moreover, the treatment effects of PD enhanced after the addition of UCG. Histological analysis of the kidney was performed using HE staining and Masson staining. Compared with the Sham group, rats in the Model group showed enlarged renal tubule lumen, vacuolation of tubular epithelial cells, interstitial dilatation, and focal renal fibrosis (Figure 1C and D). PD treatment significantly inhibited the occurrence of renal lesions. The addition of UCG further enhanced the therapeutic effect of PD. Compared with the Sham group, the concentrations of BUN, Scr, Cre, and UPr in the Model group increased, while the Ccr decreased. Moreover, compared with the Model group, the concentrations of BUN, Scr, Cre and UPr in PD group decreased, and Ccr increased. The concentrations of BUN, Scr and UPr in the UCG group were lower than those in the PD group, and the value of Ccr was higher (Figure 1E). Our results suggested that UCG treatment improved renal function in ESRD rats. As can be seen from Figure 1F, compared with the Model group, the levels of inflammatory factors (TNFα, IL1β, IL-5, IL-6) in the PD group were decreased, while those in the UCG group were lower than those in the PD group. In summary, UCG alleviated symptoms in ESRD rats.

UCG Inhibited p38 MAPK/NF-κB Signaling Pathway in Rat Kidneys

Then, to investigate the effect of UCG on the metabolic pathway of the rat kidney, qRT-PCR, WB, and IHC were probed to reveal the expression levels of P65 and P38 in renal tissues. As can be seen from Figure 2A–C, the expression levels of
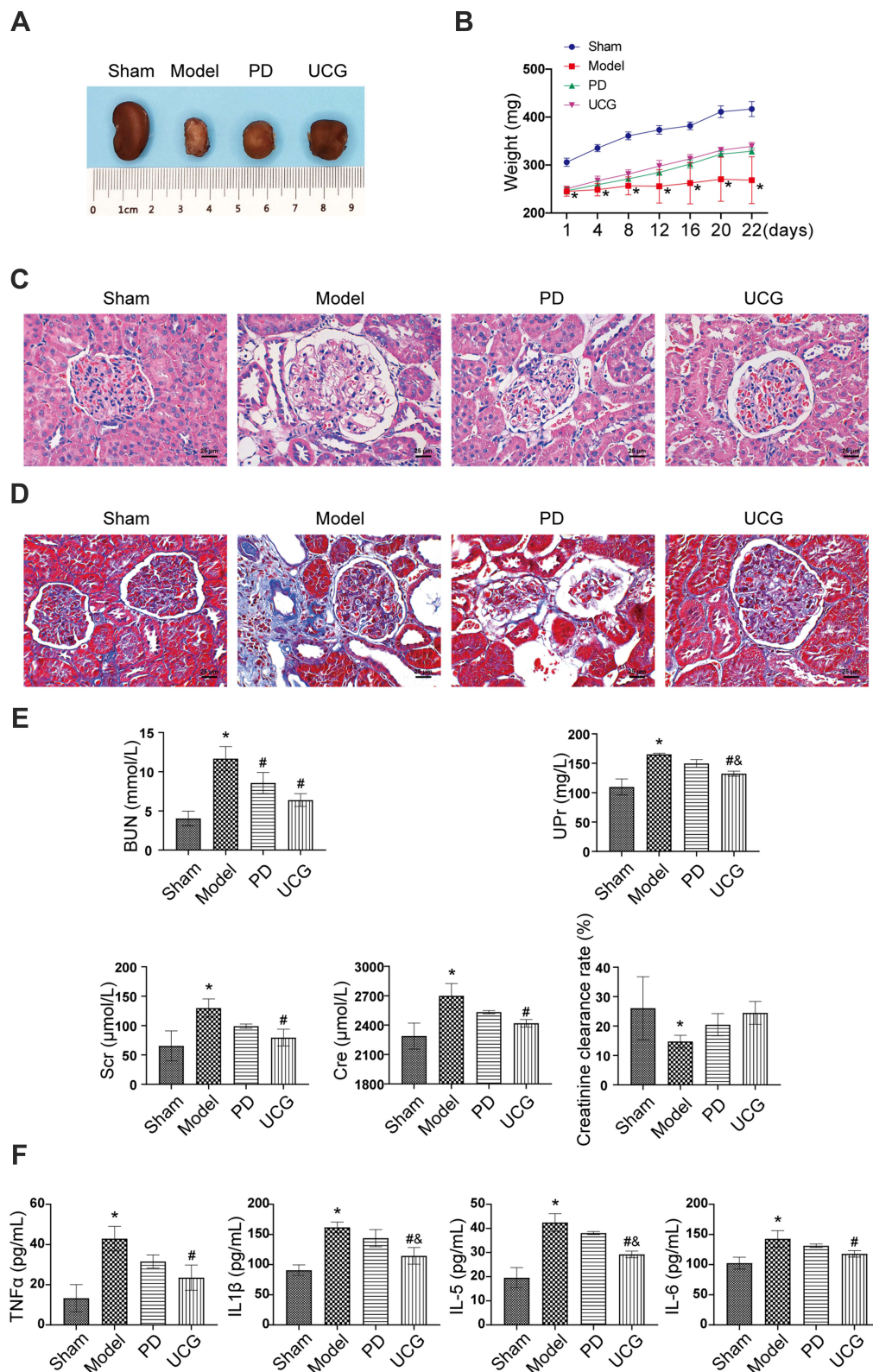
Figure 1 UCG alleviated the symptoms of ESRD rats.
Notes: (**A**) The kidney of rats after different treatment. (**B**) Changes in body weight in rats. (**C**) HE staining was used to observe the morphology of renal tissue in rats. (**D**) Masson staining was applied to detect the expression of collagen in the renal tissue of rats. (**E**) The concentrations of BUN, Scr, and UPr in were determined by ELISA, and Ccr was calculated. (**F**) The concentration of inflammatory cytokines in the serum of rats was tested by ELISA. The magnification is 400 times, scale bar = 25 μm; *$P<0.05$ compared with the Sham group. #$P<0.05$ compared with the Model group. &$P<0.05$ compared with the PD group.
Abbreviations: ESRD, end-stage renal disease; UCG, Uremic Clearance Granules; Scr, serum creatinine; Ccr, creatinine clearance rate; HE, hematoxylin-eosin; ELISA, enzyme-linked immunosorbent assay; BUN, urea nitrogen; UPr, urinary protein; CRE, creatinine.
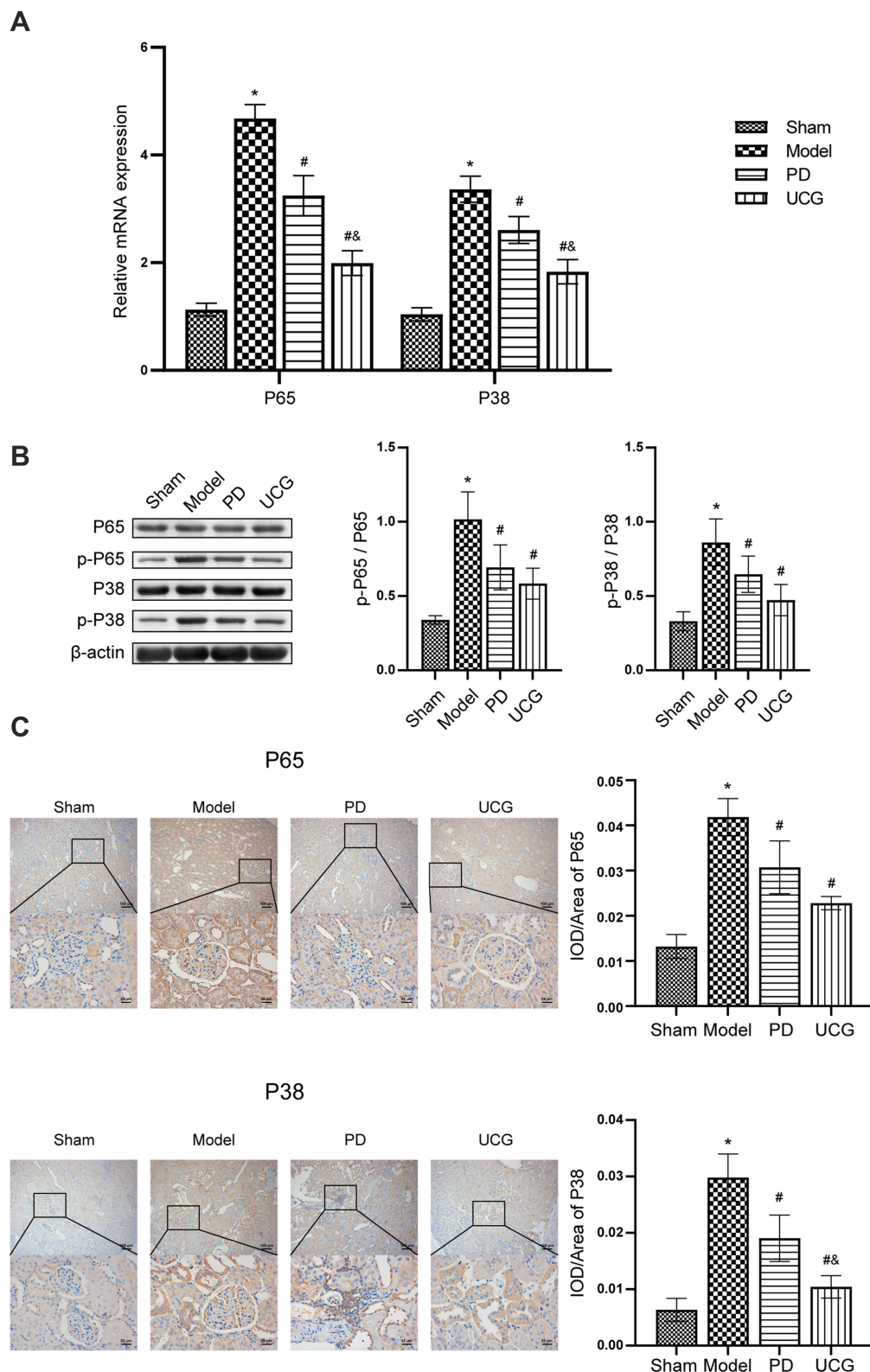
Figure 2 UCG inhibited NF-κB and MAPK signaling pathways in rat kidneys.
Notes: (**A**) The relative expression levels of P65 and P38 were detected by qRT-PCR. (**B**) The P65, P38, p-P65, and p-P38 expressions were measured by WB. (**C**) IHC examined the expression levels of P65 and P38. The magnification is 400 times, scale bar = 25 μm; *P<0.05 compared with the Sham group. #P<0.05 compared with the Model group. &P<0.05 compared with the PD group.
Abbreviations: UCG, Uremic Clearance Granules; MAPK, mitogen-activated kinase; NF-κB, nuclear factor kappa B; HE, hematoxylin-eosin; WB, Western blot.

P65 and P38 were significantly increased in the Model group compared with the Sham group. Compared with the Model group, the expression levels of P65 and P38 were decreased in the PD group. When UCG treatment was added to PD, the expression of P65 and P38 levels were further decreased. These results indicated that UCG could inhibit the expression and activation of the p38 MAPK/NF-κB signaling pathway in rat kidneys.

UCG Inhibited p38 MAPK/NF-κB Signaling Pathway in Colon Tissues of ESRD Rats

To investigate whether UCG could affect the metabolism of colon tissue in ESRD rats, we detected the expression of P65 and P38 in colon tissue. Compared with the Sham group, the expression levels of P65 and P38 levels were significantly increased in the Model group (Figure 3A–C). After PD treatment, P65 and P38 expression levels were decreased. UCG enhanced the therapeutic effect of PD. These results suggested that UCG inhibited the expression and activation of p38 MAPK/NF-κB signaling pathway in the colon tissues of ESRD rats.

UCG Improved the Relative Abundance of Some Gut Microbiota in ESRD Rats

16S rDNA sequencing technology was performed to calculate the structure of gut microbiota in rats. Figure 4A showed the number of common and unique ASV in each group. The number and species of gut microbiota in the four groups all showed great differences. g_D_5_uncultured_bacterium_F_D_4_Muribaculaceae, and g_D_5_Lachnospiraceae_NK4A136_group were dominant among the 20 genera with the highest relative abundance (Figure 4B). The rarefaction curve constructed based on the Observed ASVs number was used to describe the situation in the species increasing with the increase of sample size. As represented by the rarefaction curve of the Chao1 index (Figure 4C), the end of the curve gradually flattened out, indicating that the sample size was sufficient. As shown in Figure 4D, Observe, Chao1 and ACE indexes were used to reflect flora richness, while Shannon, Simpson, and J indexes reflected microbiota diversity. Interestingly, compared with the Sham group, the richness and diversity of the microbiota in the Model group did not change significantly. In contrast, the richness and diversity of the microbiota in the PD group and the UCG group decreased.

Anosim was used to analyze the significance of the difference. As can be seen from Figure 5A: R=0.285, P=0.001. This suggested the inter-group difference of the four groups was greater than the intra-group difference. It proved that grouping makes sense. Figure 5B showed the abundance differences between groups of the 20 genera with the largest relative abundance. Compared with the Sham group, the relative abundance of Uncultured_Bacterium_F_D_4_Muribaculaceae in Bacteroidetes phylum in the Model group was significantly increased, and no significant improvement was seen after PD treatment, and that in the UCG group decreased (Figure 5C). Meanwhile, compared with the Sham group, the relative abundance of Lachnospiraceae_NK4A136_group in the Firmicutes phylum in the Model group decreased. At the same time, the PD group and UCG group increased their relative abundance (although these changes were not significant). 16S rDNA sequencing results exhibited that UCG could reverse the aberrant relative abundance of some dominant strains in ESRD rats.

UCG Improved the Metabolic Level of ESRD Rats

LC-MS analyzed the metabolic profiles of rat serum samples. PCA analysis was an unsupervised multi-dimensional statistical analysis method that can reflect the overall metabolic differences between each group of samples and the variation degree between samples within the group as a whole. As seen in Figure 6A, the composition of the metabolome in the Model group was significantly different from the Sham group. After PD treatment, the structure of the metabolome was similar to that of the Sham group. The metabolome structure of the UCG group was most similar to that of the Sham group. PLS-DA was a multivariate statistical analysis method with supervised pattern recognition. The multi-dimensional data were grouped according to the different factors that needed to be searched before compression. In this way, the variables that were most relevant to the grouping factors could be found, and the influence of some other factors reduced. As shown in Figure 6B, the 4 groups were significantly separated, indicating that the differences between groups were greater than those within groups. Then, the different metabolites between groups were normalized for clustering analysis and presented with a heat map. A total of 70 differential metabolites were screened. Most of the metabolites were related to amino acid metabolism. Compared with the Sham group, the contents of L-glutamine (C00064), D-glutamine (C00819), L-phenylalanine (C00079), and L-tyrosine (C00082) in the Model group decreased. However, Hippurate (C01586) was increased in the Model group (Figure 6C). After PD and UCG treatment, the expression levels of these
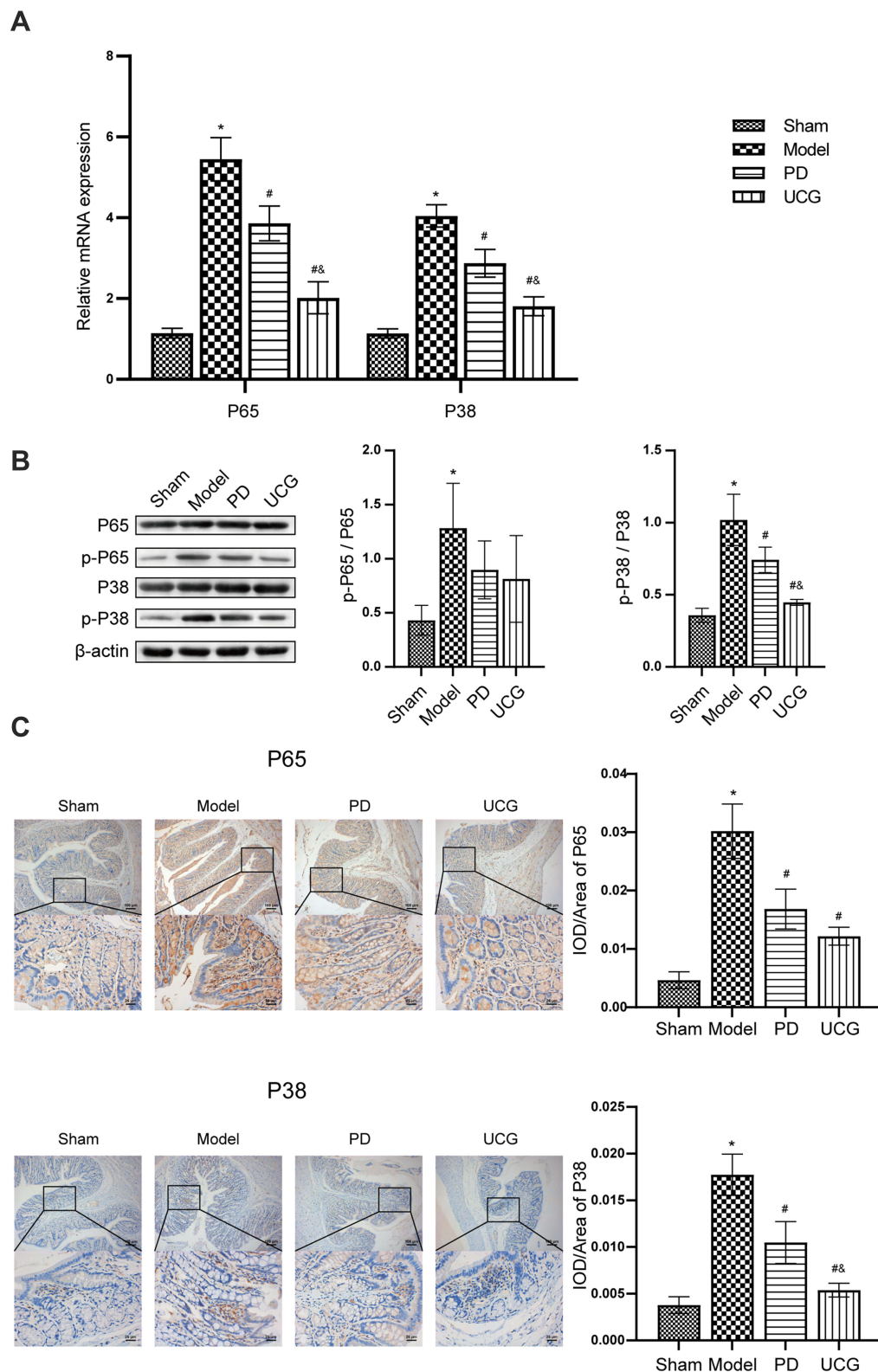
Figure 3 UCG inhibited NF-κB and MAPK signaling pathways in colon tissues of rats.
Notes: (**A**) The relative expression levels of P65 and P38 were detected by qRT-PCR. (**B**) The P65, P38, p-P65, and p-P38 expressions were measured by WB. (**C**) IHC examined the expression levels of P65 and P38. The magnification is 400 times, scale bar = 25 μm; *P<0.05 compared with the Sham group. #P<0.05 compared with the Model group. &P<0.05 compared with the PD group.
Abbreviations: UCG, Uremic Clearance Granules; MAPK, mitogen-activated kinase; NF-κB, nuclear factor kappa B; WB, Western blot.
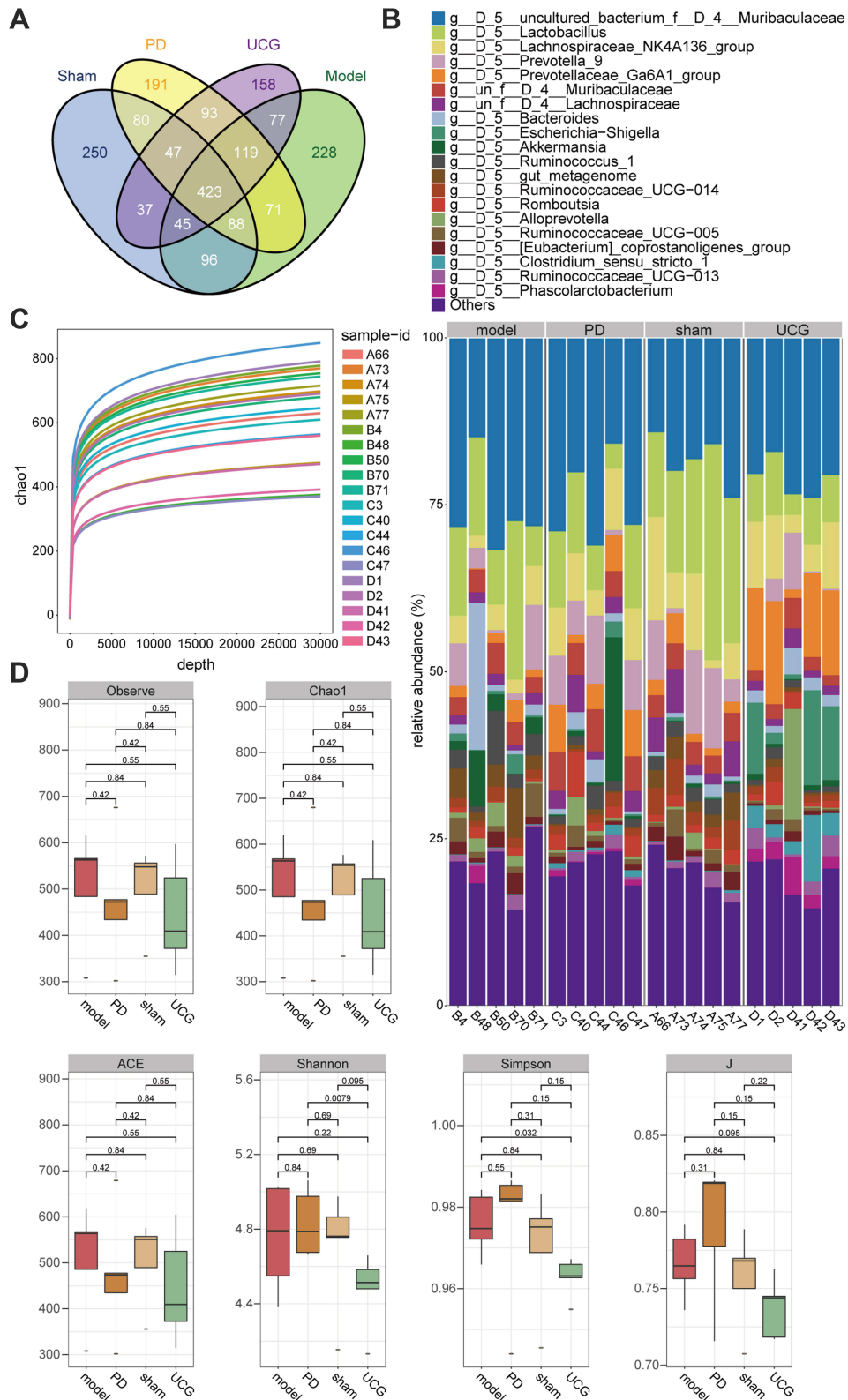
Figure 4 UCG improved the relative abundance of some gut microbiota in ESRD rats receiving PD.
Notes: (**A**) Differences in the number of ASV in the four groups. (**B**) The relative abundance of the 20 genera with the largest relative abundance. (**C**) Rarefaction curve of Chao1 index. (**D**) Alpha diversity in four groups.
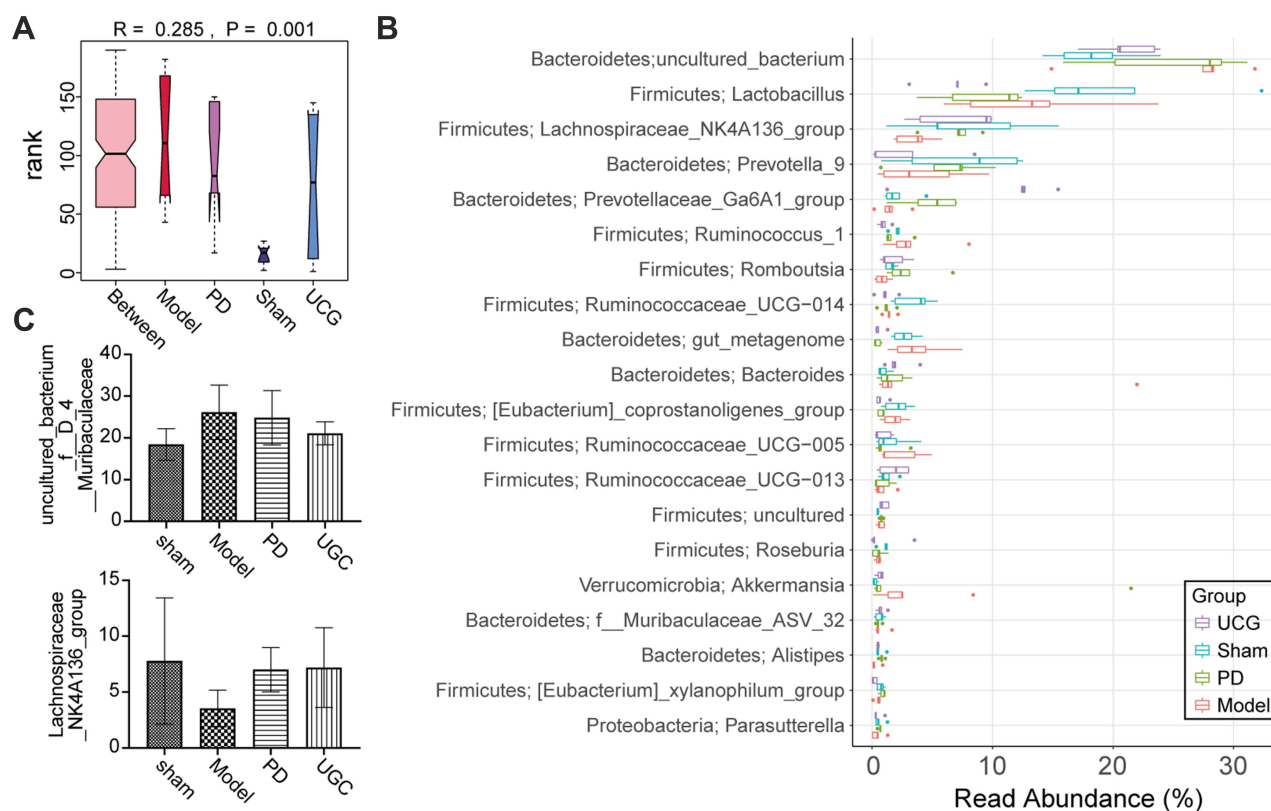**Abbreviations**: ESRD, end-stage renal disease; UCG, Uremic Clearance Granules.

Figure 5 UCG improved the relative abundance of some gut microbiota in ESRD rats (β diversity).
Notes: (**A**) Anosim detected differences in beta diversity among the four groups. (**B**) The abundance difference of the 20 genera with the largest relative abundance. (**C**) The relative abundance of uncultured_Bacterium_f_D_4_Muribaculaceae and Lachnospiraceae_NK4A136_group.
Abbreviation: UCG, Uremic Clearance Granules.

differential metabolites were closer to the Sham group. Finally, the Kyoto Encyclopedia of Genes and Genomes (KEGG) pathway (https://www.kegg.jp/kegg/pathway.html) was applied to predict the functions of the difference in the serum metabolites. As shown in Figure 6D, Phenylalanine, tyrosine and tryptophan biosynthesis, D-glutamine and D-glutamate metabolism were detected in the 23 enriched pathways. Phenylalanine metabolism had the highest enrichment rate. These results revealed that PD and UCG improved the metabolic level of ESRD rats.

Discussion

UCG was made from various Chinese herbal medicines such as rhubarb, astragalus membranaceus, white mulberry bark, sophora flavescens and Atractylodes atractylodes. According to LC-MS detection, UCG contains hundreds of compounds, mainly glycyrrhizic acid ammonium salt, Albiflorin, paeoniflorin, and 2,3,5,4 '- tetrahydroxystilbene-2-o- β-D-glucoside (TSG). Among them, glycyrrhizic acid ammonium salt was a derivative of glycyrrhizin and had anti-inflammatory and anti-allergic effects.[24] Albiflorin was isolated from peony root and had anti-inflammatory and immunomodulatory effects.[25] Albiflorin could reverse the increase triglycerides, cholesterol, plasma aspartate amino-transferase, and TNFα levels in the liver.[26] Paeoniflorin was a water-soluble monoterpene glycoside which isolated from the peony. It had a wide range of medicinal properties, including anti-inflammatory, anti-oxidant, anti-thrombosis, anti-tumor, etc.[27] Paeoniflorin regulated the function and activation of immune cells, reduced the production of inflammatory mediators, and restored the abnormally expressed MAPK/NF-κB pathway.[28] TSG was one of the active ingredients extracted from Polygonum multiflorum and was an anti-oxidant.[29] TSG inhibited pro-inflammatory factors by attenuating NF-κB binding activity in microglia.[30] In summary, UCG might slow the progression of ESRD by regulating NF-κB to reduce the expression of inflammatory factors and alter the intestinal microbiome and its metabolism.
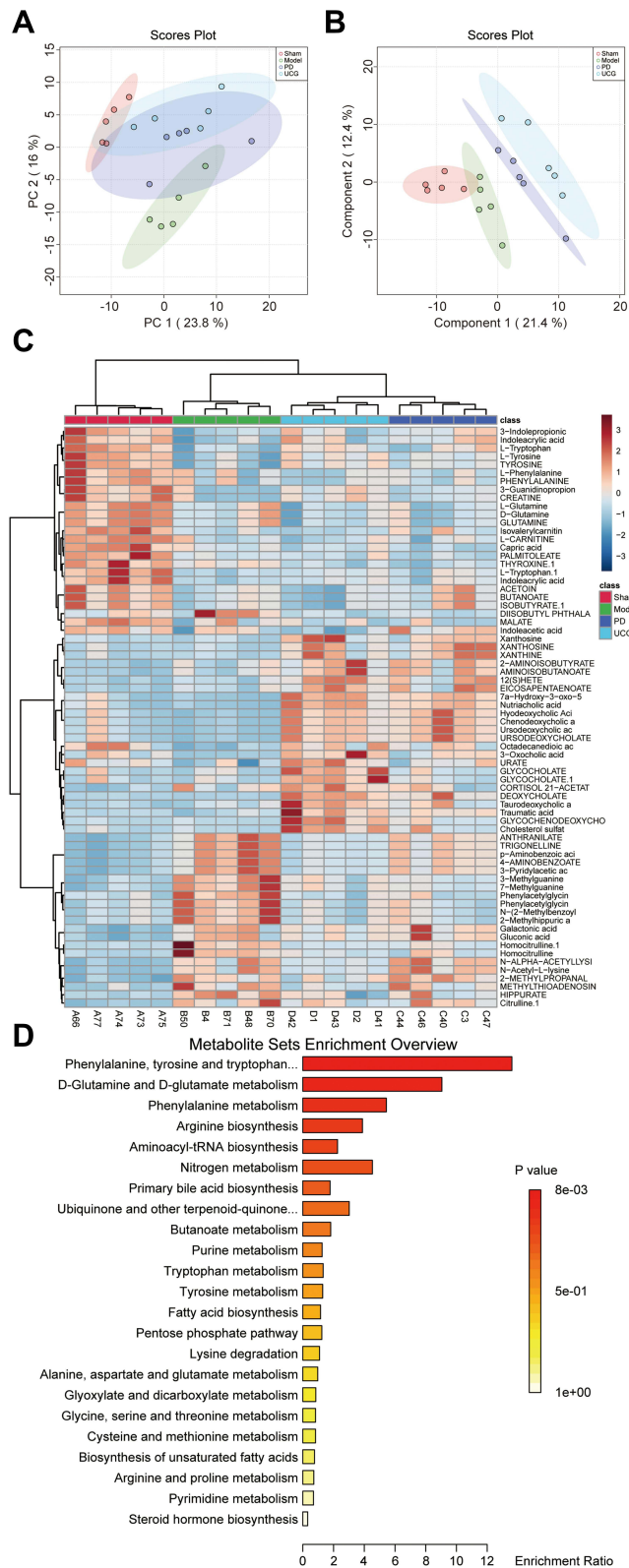
Figure 6 UCG improved the metabolic level of ESRD rats.
Notes: (**A**) PCA performed dimensionality reduction analysis on the metabolome data. (**B**) PLS-DA was used to analyze the metabolome data. (**C**) The expression of 80 differentially expressed metabolites in 4 groups. (**D**) KEGG was applied for functional annotation of differentially expressed metabolites.
Abbreviations: ESRD, end-stage renal disease; UCG, Uremic Clearance Granules; KEGG, Kyoto Encyclopedia of Genes and Genomes.

In this study, the 5/6 Nx rat models were established to investigate the therapeutic effect of UCG on ESRD rats. We found that UCG improved renal tubule lumen enlargement, tubular epithelial vacuolation, interstitial dilatation, and focal renal fibrosis in ESRD rats. These were the common pathophysiology of nephropathy. For example, ablation of autophagy-related genes in proximal renal tubules resulted in autophagy deficiency and more severe renal hypertrophy, tubular damage, inflammation, and fibrosis in diabetic mice.[31] A significant decrease in BUN, Scr and other renal function indexes indicated renal failure.[32] We observed that the BUN, Scr, Cre, and UPr in the Model group significantly increased. The treatment of PD decreased these indicators, while UCG treatment enhanced the effect of PD treatment. In addition, the level of KI decreased significantly in the Model group but increased in the PD and UCG groups. In other words, UCG could improve renal tissue structure and enhance renal function in ESRD rats treated with PD.

Next, we studied the changes of p38 MAPK/NF-κB signaling pathway in renal and colon tissues of rats at the molecular level. Phosphorylation level represented the activity of p38 MAPK/NF-κB signaling pathway.[33] Our study found that the expression and activation levels of p65 NF-κB and p38 MAPK were increased abnormally in the Model group, and PD treatment improved this situation. UCG treatment further reduced the expression and activation levels of p65 NF-κB and p38 MAPK. Similarly, Tripterygium wilfordii and its extract could also regulate p38 MAPK, NF-κB, TGF-β, Wnt/ β-catenin pathways in treating diabetic nephropathy efficacy and pharmacological mechanism.[34] Astaxanthin could target various diseases, such as nervous system diseases, diabetes, gastrointestinal diseases, liver, and kidney diseases, through the inflammatory mechanisms regulated by NF-κB and MAPK pathways.[35] The development of CKD affects the composition of the gut microbiome, which in turn affects the level of gut metabolism.[36] Our study confirmed that UCG could improve the abnormal expression and activation of p38 MAPK/ NF-κB pathways in renal tissues of ESRD rats, and extend its effect to colon tissues.

By 16S rDNA sequencing, we found that Bacteroidetes were dominant in ESRD rats. It has been reported that the mammalian gut microbiota can be divided into two groups according to the dominant species: intestinal type 1 is dominated by Bacteroidetes, which metabolize protein, while intestinal type 2 mainly contains sugar-soluble Preverella.[37] In this study, the different gut microbiota in ESRD rats was mainly concentrated in Bacteroidetes uncultured_Bacterium_F_D_4_Muribaculaceae and Firmicutes lachnospiraceae_NK4A136_group. Lai et al suggested that BSA aggravated kidney injury by altering the relative abundance of the Muribaculaceae genus in the mouse gut microbiota, causing immune activation and chronic inflammation.[38] The relative abundance of Lachnospiraceae_NK4A136_group changed significantly in the gut microorganism of adult kidney disease and kidney stones.[39] We found that PD and UCG treatment had no significant effect on improving gut microbiota diversity in ESRD rats. However, PD and UCG improved the relative abundance of some of the different flora (although the difference was not significant).

We have previously demonstrated that the gut microbiota of ESRD rats was altered. These changes influenced the development of the disease by modulating the metabolite profile in the gut.[40] In the serum metabolome of rats, we found that the contents of L-glutamine and D-glutamine in ESRD rats were significantly decreased, and D-glutamine and D-glutamate metabolic pathway showed significant differences. Glutamine is the most abundant and versatile amino acid in the body. It has two configurations: D-glutamine and L-glutamine.[41] The main end-products of glutamine metabolism are glutamic acid, aspartic acid, carbon dioxide and ammonia.[42] In vitro and in vivo studies have identified glutamine as an essential nutrient for lymphocyte proliferation and cytokine production, macrophage phagocytosis and secretion, and neutrophil killing.[43] In intestinal physiology, glutamine promotes intestinal cell proliferation, regulates tight junction proteins, inhibits pro-inflammatory signaling pathways, and protects cells from apoptosis and cellular stress under normal and pathological conditions.[44] In the "Introduction" section, we have mentioned that the development of ESRD was associated with an active inflammatory response. In other words, the rapid depletion of glutamine made the active inflammatory response unable to be effectively suppressed, leading to the rapid development of ESRD. Fortunately, PD and UCG treatment can inhibit the deterioration of ESRD.

Our study found that the phenylalanine metabolic pathway was significantly changed in the serum metabolome of ESRD rats. For instance, the contents of L-phenylalanine and L-tyrosine were decreased, while the content of hippurate was increased. After PD and UCG treatment, phenylalanine metabolism gradually approached the normal level. Phenylalanine hydroxylase used tetrahydrotrexate and oxygen to hydroxyl phenylalanine in the liver to tyrosine.[45] Tyrosine was used in the biosynthesis of protein, biogenic amines, and melanin, or catabolized to energy by five enzymatic reactions to produce acetoacetate and fumarate.[46] If CKD was associated with impaired renal function,

several uremia solutes were retained; Some of these produce toxic effects called uremia toxins.[47] Hippurate was a uremia toxin that can be produced by anaerobic bacteria, especially Clostridium, using aromatic amino acids such as L-phenylalanine, L-tyrosine, or L-tryptophan.[48] Therefore, it is reasonable to speculate that UCG could slow down the accumulation of toxins in ESRD by regulating phenylalanine metabolism.

As validated by clinical samples, previous studies have shown that ESRD-related Diabetic kidney disease was significantly associated with phenylalanine metabolism [PMID: 34899312]. Due to time and funding constraints, we only did preliminary research on metabolomics. In the future, we will further study the in-depth study of UCG on the mechanism of intestinal metabolism in rats. In the future, we are expected to regulate ESRD progression by modulating phenylalanine metabolism in humans.

Conclusion

UCG could inhibit the expression and activation of p38 MAPK/ NF-κB signaling pathway, improve the relative abundance of some gut microbiota, and regulate D-glutamine and D-glutamate metabolism, and Phenylalanine metabolism. Thus, the therapeutic effect of PD on ESRD rats was enhanced. This finding advanced the understanding of the pathogenesis of ESRD and was expected to improve clinical outcomes in patients with ESRD.

Acknowledgments

Disclosure

The authors report no conflicts of interest in this work.

References

1. Han E, Shiraz F, Haldane V, et al. Biopsychosocial experiences and coping strategies of elderly ESRD patients: a qualitative study to inform the development of more holistic and person-centred health services in Singapore. *BMC Public Health*. 2019;19(1):1107. doi:10.1186/s12889-019-7433-6

2. Xie J, Zeng S, Xie L, et al. Differences in the clinical presentation, management, and in-hospital outcomes of acute aortic dissection in patients with and without end-stage renal disease. *BMC Nephrol*. 2021;22(1):257. doi:10.1186/s12882-021-02432-9

3. Perl J, McArthur E, Tan VS, et al. ESRD among immigrants to Ontario, Canada: a population-based study. *J Am Soc Nephrol*. 2018;29(7):1948–1959. doi:10.1681/ASN.2017101055

4. Mehrotra R, Devuyst O, Davies SJ, Johnson DW. The current state of peritoneal dialysis. *J Am Soc Nephrol*. 2016;27(11):3238–3252. doi:10.1681/ASN.2016010112

5. Miao XH, Wang CG, Hu BQ, Li A, Chen CB, Song WQ. TGF-beta1 immunohistochemistry and promoter methylation in chronic renal failure rats treated with Uremic Clearance Granules. *Folia Histochem Cytobiol*. 2010;48(2):284–291. doi:10.2478/v10042-010-0001-7

6. Huang YR, Wei QX, Wan YG, et al. Ureic clearance granule, alleviates renal dysfunction and tubulointerstitial fibrosis by promoting extracellular matrix degradation in renal failure rats, compared with enalapril. *J Ethnopharmacol*. 2014;155(3):1541–1552. doi:10.1016/j.jep.2014.07.048

7. Lu ZY, Liu SW, Xie YS, et al. Inhibition of the tubular epithelial-to-mesenchymal transition in vivo and in vitro by the Uremic Clearance Granule (). *Chin J Integr Med*. 2013;19(12):918–926. doi:10.1007/s11655-013-1654-9

8. Wu HM, Sun HJ, Wang F, Yang M, Dong BR, Liu GJ. Oral adsorbents for preventing or delaying the progression of chronic kidney disease. *Cochrane Database Syst Rev*. 2014;(10):Cd007861. doi:10.1002/14651858.CD007861.pub2

9. Romero-Becerra R, Santamans AM, Folgueira C, Sabio G. p38 MAPK pathway in the heart: new insights in health and disease. *Int J Mol Sci*. 2020;21(19):7412. doi:10.3390/ijms21197412

10. Ghoneum A, Said N. PI3K-AKT-mTOR and NFκB pathways in ovarian cancer: implications for targeted therapeutics. *Cancers (Basel)*. 2019;11(7):949. doi:10.3390/cancers11070949

11. Xing S, Zhang B, Hua R, et al. URG4/URGCP enhances the angiogenic capacity of human hepatocellular carcinoma cells in vitro via activation of the NF-κB signaling pathway. *BMC Cancer*. 2015;15:368. doi:10.1186/s12885-015-1378-7

12. Nie Y, Wang Z, Chai G, et al. Dehydrocostus lactone suppresses LPS-induced acute lung injury and macrophage activation through NF-κB signaling pathway mediated by p38 MAPK and Akt. *Molecules*. 2019;24(8):1510. doi:10.3390/molecules24081510

13. Liu Z, Zhong T, Zheng D, Cepinskas I, Peng T, Su L. Heat stress pretreatment decreases lipopolysaccharide-induced apoptosis via the p38 signaling pathway in human umbilical vein endothelial cells. *Mol Med Rep*. 2016;14(1):1007–1013. doi:10.3892/mmr.2016.5303

14. Wu D, Luo N, Wang L, et al. Hydrogen sulfide ameliorates chronic renal failure in rats by inhibiting apoptosis and inflammation through ROS/ MAPK and NF-κB signaling pathways. *Sci Rep*. 2017;7(1):455. doi:10.1038/s41598-017-00557-2

15. Jiang J, Zheng D, Li Y, Liu G, Zhou H, Liu Y. Long noncoding RNA MANTIS relieved the protein-bound uremic toxin-induced injury on human umbilical vein endothelial cells in chronic kidney disease and end-stage renal disease. *Int J Clin Exp Pathol*. 2018;11(7):3236–3246.

16. Liu Y. Cellular and molecular mechanisms of renal fibrosis. *Nat Rev Nephrol*. 2011;7(12):684–696. doi:10.1038/nrneph.2011.149

17. Mo L, Xiao X, Song S, et al. Protective effect of Huang Gan formula in 5/6 nephrectomized rats by depressing the Wnt/β-catenin signaling pathway. *Drug Des Devel Ther*. 2015;9:2867–2881. doi:10.2147/DDDT.S81157

18. Evenepoel P, Poesen R, Meijers B. The gut-kidney axis. *Pediatr Nephrol*. 2017;32(11):2005–2014. doi:10.1007/s00467-016-3527-x

19. Zhao J, Ning X, Liu B, Dong R, Bai M, Sun S. Specific alterations in gut microbiota in patients with chronic kidney disease: an updated systematic review. *Ren Fail*. 2021;43(1):102–112. doi:10.1080/0886022X.2020.1864404

20. Vaziri ND, Wong J, Pahl M, et al. Chronic kidney disease alters intestinal microbial flora. *Kidney Int*. 2013;83(2):308–315. doi:10.1038/ki.2012.345

21. Jiang S, Xie S, Lv D, et al. Alteration of the gut microbiota in Chinese population with chronic kidney disease. *Sci Rep*. 2017;7(1):2870. doi:10.1038/s41598-017-02989-2

22. Wei X, Bao Y, Zhan X, et al. MiR-200a ameliorates peritoneal fibrosis and functional deterioration in a rat model of peritoneal dialysis. *Int Urol Nephrol*. 2019;51(5):889–896. doi:10.1007/s11255-019-02122-4

23. Zhang Y, Wang L, Meng L, Cao G, Wu Y. Sirtuin 6 overexpression relieves sepsis-induced acute kidney injury by promoting autophagy. *Cell Cycle*. 2019;18(4):425–436. doi:10.1080/15384101.2019.1568746

24. Barone A, Cristiano MC, Cilurzo F, et al. Ammonium glycyrrhizate skin delivery from ultradeformable liposomes: a novel use as an anti-inflammatory agent in topical drug delivery. *Colloids Surf B Biointerfaces*. 2020;193:111152. doi:10.1016/j.colsurfb.2020.111152

25. Cai Z, Liu J, Bian H, Cai J. Albiflorin alleviates ovalbumin (OVA)-induced pulmonary inflammation in asthmatic mice. *Am J Transl Res*. 2019;11 (12):7300–7309.

26. Zhou X, Fouda S, Zeng XY, et al. Characterization of the therapeutic profile of albiflorin for the metabolic syndrome. *Front Pharmacol*. 2019;10:1151. doi:10.3389/fphar.2019.01151

27. Zhou YX, Gong XH, Zhang H, Peng C. A review on the pharmacokinetics of paeoniflorin and its anti-inflammatory and immunomodulatory effects. *Biomed Pharmacother*. 2020;130:110505. doi:10.1016/j.biopha.2020.110505

28. Zhang L, Wei W. Anti-inflammatory and immunoregulatory effects of paeoniflorin and total glucosides of paeony. *Pharmacol Ther*. 2020;207:107452. doi:10.1016/j.pharmthera.2019.107452

29. Zhang L, Chen J. Biological effects of tetrahydroxystilbene glucoside: an active component of a rhizome extracted from polygonum multiflorum. *Oxid Med Cell Longev*. 2018;2018:3641960. doi:10.1155/2018/3641960

30. Huang C, Wang Y, Wang J, Yao W, Chen X, Zhang W. TSG (2,3,4',5-tetrahydroxystilbene 2-O-β-D-glucoside) suppresses induction of pro-inflammatory factors by attenuating the binding activity of nuclear factor-κB in microglia. *J Neuroinflammation*. 2013;10:129. doi:10.1186/1742-2094-10-129

31. Ma Z, Li L, Livingston MJ, et al. p53/microRNA-214/ULK1 axis impairs renal tubular autophagy in diabetic kidney disease. *J Clin Invest*. 2020;130(9):5011–5026. doi:10.1172/JCI135536

32. Zhang G, Cui G, Tong S, Cao Q. Salvianolic acid A alleviates the renal damage in rats with chronic renal failure. *Acta Cir Bras*. 2019;34(2): e201900204. doi:10.1590/s0102-8650201900204

33. Kim DC, Quang TH, Oh H, Kim YC. Steppogenin isolated from cudrania tricuspidata shows antineuroinflammatory effects via NF-κB and MAPK pathways in LPS-stimulated BV2 and primary rat microglial cells. *Molecules*. 2017;22(12):2130. doi:10.3390/molecules22122130

34. Huang WJ, Liu WJ, Xiao YH, et al. Tripterygium and its extracts for diabetic nephropathy: efficacy and pharmacological mechanisms. *Biomed Pharmacother*. 2020;121:109599. doi:10.1016/j.biopha.2019.109599

35. Chang MX, Xiong F. Astaxanthin and its effects in inflammatory responses and inflammation-associated diseases: recent advances and future directions. *Molecules*. 2020;25(22):5342. doi:10.3390/molecules25225342

36. Giordano L, Mihaila SM, Eslami Amirabadi H, Masereeuw R. Microphysiological systems to recapitulate the gut-kidney axis. *Trends Biotechnol*. 2021;39:811–823. doi:10.1016/j.tibtech.2020.12.001

37. Yang T, Richards EM, Pepine CJ, Raizada MK. The gut microbiota and the brain-gut-kidney axis in hypertension and chronic kidney disease. *Nat Rev Nephrol*. 2018;14(7):442–456. doi:10.1038/s41581-018-0018-2

38. Lai L, Li Y, Liu J, et al. Bovine serum albumin aggravates macrophage M1 activation and kidney injury in heterozygous Klotho-deficient mice via the gut microbiota-immune axis. *Int J Biol Sci*. 2021;17(3):742–755. doi:10.7150/ijbs.56424

39. Stanford J, Charlton K, Stefoska-Needham A, Ibrahim R, Lambert K. The gut microbiota profile of adults with kidney disease and kidney stones: a systematic review of the literature. *BMC Nephrol*. 2020;21(1):215. doi:10.1186/s12882-020-01805-w

40. Kato T, Yamazaki K, Nakajima M, et al. Oral administration of porphyromonas gingivalis alters the gut microbiome and serum metabolome. *mSphere*. 2018;3(5). doi:10.1128/mSphere.00460-18

41. Kim H. Glutamine as an immunonutrient. *Yonsei Med J*. 2011;52(6):892–897. doi:10.3349/ymj.2011.52.6.892

42. Brand K. Glutamine and glucose metabolism during thymocyte proliferation. Pathways of glutamine and glutamate metabolism. *Biochem J*. 1985;228(2):353–361. doi:10.1042/bj2280353

43. Cruzat V, Macedo Rogero M, Noel Keane K, Curi R, Newsholme P. Glutamine: metabolism and immune function, supplementation and clinical translation. *Nutrients*. 2018;10(11):1564. doi:10.3390/nu10111564

44. Kim MH, Kim H. The roles of glutamine in the intestine and its implication in intestinal diseases. *Int J Mol Sci*. 2017;18(5). doi:10.3390/ijms18051051

45. Zhang S, Fitzpatrick PF. Identification of the allosteric site for phenylalanine in rat phenylalanine hydroxylase. *J Biol Chem*. 2016;291(14):7418–7425. doi:10.1074/jbc.M115.709998

46. Sterkel M, Oliveira PL. Developmental roles of tyrosine metabolism enzymes in the blood-sucking insect Rhodnius prolixus. *Proc Biol Sci*. 2017;284:1854.

47. Gryp T, Vanholder R, Vaneechoutte M, Glorieux G. p-cresyl sulfate. *Toxins (Basel)*. 2017;9(2):52. doi:10.3390/toxins9020052

48. Jaskiw GE, Obrenovich ME, Kundrapu S, Donskey CJ. Changes in the serum metabolome of patients treated with broad-spectrum antibiotics. *Pathog Immun*. 2020;5(1):382–418. doi:10.20411/pai.v5i1.394